JGR Solid Earth

RESEARCH ARTICLE
10.1029/2020JB019663

Shallow Basin Structure and Attenuation Are Key to Predicting Long Shaking Duration in Los Angeles Basin

Voon Hui Lai[1,2], Robert W. Graves[3], Chunquan Yu[4], Zhongwen Zhan[1], and Don V. Helmberger[1†]

[1]Seismological Laboratory, California Institute of Technology, Pasadena, CA, USA, [2]Research School of Earth Sciences, Australian National University, Acton, ACT, Australia, [3]U.S. Geological Survey, Pasadena, CA, USA, [4]Department of Earth Space Sciences, Southern University of Science and Technology, Shenzhen, China

†Deceased 13 August 2020

Key Points:
- Shallow earthquakes generate long shaking duration in the Los Angeles basin, which is not adequately captured by current 3-D velocity models
- Beamforming analysis shows that most of the coherent arrivals propagate along great circle paths, excited by the basin edges
- Improved descriptions of shallow basin structure and attenuation model are crucial in predicting the observed long shaking duration

Supporting Information:
- Supporting Information S1

Correspondence to:
V. H. Lai,
voonhui.lai@anu.edu.au

Citation:
Lai, V. H., Graves, R. W., Yu, C., Zhan, Z., & Helmberger, D. V. (2020). Shallow basin structure and attenuation are key to predicting long shaking duration in Los Angeles Basin. *Journal of Geophysical Research: Solid Earth*, *125*, e2020JB019663. https://doi.org/10.1029/2020JB019663

Received 26 FEB 2020
Accepted 26 SEP 2020
Accepted article online 30 SEP 2020

Abstract Ground motions in the Los Angeles Basin during large earthquakes are modulated by earthquake ruptures, path effects into the basin, basin effects, and local site response. We analyzed the direct effect of shallow basin structures on shaking duration at a period of 2–10 s in the Los Angeles region through modeling small magnitude, shallow, and deep earthquake pairs. The source depth modulates the basin response, particularly the shaking duration, and these features are a function of path effect and not site condition. Three-dimensional simulations using the CVM-S4.26.M01 velocity model show good fitting to the initial portion of the waveforms at periods of 5 s and longer but fail to predict the long shaking duration during shallow events, especially at periods less than 5 s. Simulations using CVM-H do not match the timing of the initial arrivals as well as CVM-S4.26.M01, and the strong late arrivals in the CVM-H simulation travel with an apparent velocity slower than observed. A higher-quality factor than traditionally assumed may produce synthetics with longer durations but is unable to accurately match the amplitude and phase. Beamforming analysis using dense array data further reveals the long duration surface waves have the same back azimuth as the direct arrivals and are generated at the basin edges, while the later coda waves are scattered from off-azimuth directions, potentially due to strong, sharp boundaries offshore. Improving the description of these shallow basin structures and attenuation model will enhance our capability to predict long-period ground motions in basins.

1. Introduction

Understanding the effects of sedimentary basins on ground motion is important in reducing earthquake risk for many metropolitan areas such as Los Angeles, Seattle, and Tokyo. Poorly consolidated sediments within the basin amplify ground motion, which can be severe and localized near basin edges due to strong constructive interference of seismic waves such as those observed during the 1994 Northridge and 1996 Kobe earthquakes (Graves et al., 1998; Kawase, 1996). In addition, basin structures can prolong the duration of strong shaking. Notably, the M 8.11985 Michoacán earthquake, despite occurring more than 450 km away, had an unusually long duration of long-period shaking and caused considerable damage and causalities in Mexico City which is situated on a lake-bed basin. Kawase and Aki (1989) first suggested the distinction in the mechanisms on how basins can cause ground motion amplification and long durations by showing that the prolonged shaking in Mexico City was caused by the interaction of a soft-surface layer within a deeper basin (Type-II basin) beneath the city and not by surface wave reverberation within the basin. Similarly, within the Los Angeles Basin, Saikia et al. (1994) proposed that the presence of multiple low-velocity pockets within the basin can trap and delay the surface seismic waves propagating through them, allowing the seismic energy to appear at a later time and cause prolonged strong shaking. In recent years, other ideas have been proposed to explain these shaking durations including a combination of basin reflections and mountain refractions (Lee et al., 2008) and surface wave overtones excited at the basin edge (Boué et al., 2016; Cruz-Atienza et al., 2016). The high density of stations in Kanto Basin, Japan, allowed Boué et al. (2016) to use ambient seismic field measurements to reconstruct the wavefield propagating across the basin, further highlighting the role of basin edges in exciting higher-mode surface waves. However, the mechanisms behind the prolonged shaking durations observed in the Los Angeles Basin remain difficult to investigate without dense instrumentation to adequately resolve the seismic wavefield.

The development of high-resolution three-dimensional (3-D) velocity models that include details of sedimentary basin structures, in combination with numerical modeling techniques capable of simulating waveforms accurately down to 1 s, allows us to simulate the effects of basin structures on ground motion. For the Los Angeles Basin, two Southern California Earthquake Center Community Velocity Models (CVMs), which are CVM-S4.26.M01 (Lee et al., 2014; referred as CVM-S hereafter) and CVM-H 15.1.0 (Shaw et al., 2015; referred as CVM-H hereafter), are commonly used in ground motion studies. In CVM-S, the initial basin structure is constrained using a rule-based seismic velocity model, derived primarily from well log data (Magistrale et al., 1996), in which V_P is a function of sediment age and depth. In CVM-H, basin structures are determined from sonic logs and seismic reflection profiles collected by the petroleum industry (Süss & Shaw, 2003), with an added high-resolution geotechnical layer (GTL) based on V_{S30} measurements (Ely et al., 2010) to better describe the upper few hundred meters. The models are further refined using tomographic inversions with a variety of data sets including earthquakes, ambient noise correlation, seismic reflection profiles, and receiver functions. Based on these high-resolution models, ground motion simulations of scenario earthquakes, such as TeraShake (Olsen et al., 2006) and CyberShake (Graves et al., 2011) runs, can capture the significant influence of basin structure on site amplification and waveguide channeling. In particular, shallow surface rupture from hypothetical M7+ events along the San Andreas Fault can cause strong ground motion within the greater Los Angeles area highlighting the importance of understanding the effects of shallow structures on ground motion. To validate the accuracy of the CVMs, forward simulations of recorded earthquake events have been performed (Komatitsch et al., 2004; Taborda et al., 2016), and the models are assessed based on their ability to predict the observed ground motions, with an emphasis on the ground motion spectral response.

Accurate prediction of ground motion in Los Angeles, particularly for large earthquake scenarios such as a San Andreas rupture, depends on several important factors including earthquake magnitude and rupture length, effects of the path into the Los Angeles Basin, and the local basin effects. Several studies (e.g., Day et al., 2008; Hruby & Beresnev, 2003) focused on the effect of basin depth, yet the effect of earthquake depth on basin response—ground motion amplitude and duration—remains unclear. Recent studies by Wirth et al. (2019) and Moschetti et al. (2019) challenged the notion that earthquake source and site response can be treated independently of each other and showed a strong dependence of earthquake location on basin amplification at the Seattle and Tacoma basins (Wirth et al., 2019) and Cook Inlet region, Alaska (Moschetti et al., 2019). Bowden and Tsai (2017) further showed that in basin environments, horizontally traveling surface waves can cause larger site amplification at long period (>1 s) compared to the vertically incident waves, which have strong implications for shallow earthquakes.

In this study, we find that there are similar source-dependent basin effects in the Los Angeles Basin: Shallow earthquakes preferentially amplify ground motion intensity and increase shaking duration at longer periods (2–10 s). Through studying local, small magnitude earthquakes using numerical simulations and dense array techniques, we show that improved representation of the shallow basin structures and attenuation in 3-D velocity models is key to predicting the long shaking duration.

2. Observations

To study the direct response of earthquake depth on ground motion in basins, we choose three groups of small earthquakes occurring at the basin edge at different depths (Figure 1 and Table 1). The Beverly Hills-Westwood pair and Chino Hills series sample the Los Angeles basin and have moment magnitudes between 3.2 and 3.9. The Fontana pair is larger in moment magnitude (4.3–4.4) and sample all the major regional basins including the San Bernardino, San Gabriel, and Los Angeles basins. These events are recorded by the regional Southern California Seismic Network (SCSN). The Beverly Hills event is also recorded by a temporary nodal dense array.

The focal mechanisms are constrained using the Cut-and-Paste (CAP) moment tensor inversion method (Zhao & Helmberger, 1994; Zhu & Helmberger, 1996). To determine the best focal depth, we use a grid search approach that minimizes the waveform misfit. The CAP method has since been updated to allow for 3-D Green's functions, which improves the waveform fitting of small magnitude events in the period range of 5.5 to 12.5 s, especially at stations within the basin (Wang & Zhan, 2020; Zhu & Zhou, 2016). The depths for the Beverly Hills-Westwood pair are 1.5 and 9.0 km, respectively, as determined from our grid

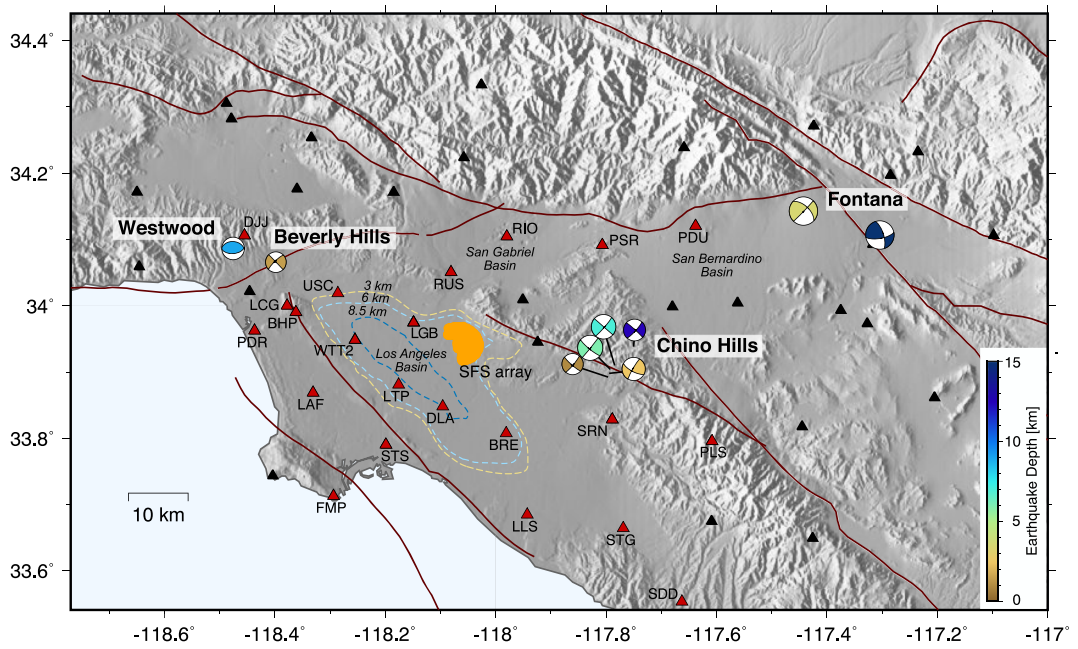

Figure 1. Map shows the location of earthquakes: the Beverly Hills-Westwood pair and Chino Hills series, directly sampling the Los Angeles basin, and the Fontana pair, sampling the San Bernardino, San Gabriel, and Los Angeles basins. The earthquakes are color coded by their depths. Triangles represent available broadband stations from the Southern California Seismic Network (CI network code). Stations highlighted in this study are colored in red. The temporary Santa Fe Springs (SFS) dense array is in orange. The contour lines outline the Los Angeles basin basement depth at 3, 6, and 8.5 km, estimated from CVMS-4.26.M01. Red lines delineate known regional faults (Jennings, 1994).

search (supporting information Figure S1), and they are similar to the depths (3.5 and 9.8 km, respectively) obtained from relocations using waveform cross-correlation (Hauksson et al., 2012). The focal mechanisms and depths of the Chino Hills series are obtained from the 3-D CAP catalog by Wang and Zhan (2020). For the Fontana pair, we use the moment tensor solutions and depths determined by Lui et al. (2016) which are used extensively in their study on rapid assessment of earthquake source properties. The earthquake parameters are listed in Table 1.

Direct comparison of the waveforms recorded by the broadband stations shows that shallow earthquakes preferentially excite stronger and longer shaking at period 2–10 s in a basin environment. Despite a smaller magnitude, the shallow Beverly Hills event shows stronger and longer shaking for stations within the Los Angeles Basin compared to that from the stronger and deeper Westwood event. This contrast in shaking duration is observed in all components (Figure 2, tangential; Figure S2, radial; and Figure S3, vertical). For the tangential component of the Beverly Hills event, we observe two prominent wave packets traveling at an apparent velocity of 1,170 and 740 m/s, with the slower packet having larger amplitude and longer period signal. The particle motions of the early and later wave packets, measured using the radial and vertical components (Figure S4), are prograde and retrograde, respectively, which often indicate the excitation of higher and fundamental-mode surface waves (Boué et al., 2016; Ma et al., 2016). As the higher-mode surface wave is sensitive to greater depths which have higher velocity, it usually travels faster than the fundamental mode. These wave packets are not observed in the deeper event.

Similarly, we observe that shallow events excite significantly longer and stronger shaking at period 2–10 s in the Chino Hills series, which share a similar strike-slip focal mechanism (Figures 3a and S5). The phenomenon becomes subdued at larger depths, when the events are located around or deeper than the Los Angeles basin basement depth (~8.5 km). The phenomenon is path dependent: Stations LAF and STS that are along the basin profile show an additional ~50 s of shaking but not SDD which has a travel path completely outside the basin (Figure 3b). The phenomenon also occurs at stations with different seismic site classification, a measure used by the geotechnical and engineering community to predict ground motion intensity based

Table 1
The Origin Time, Location, Depth, Moment Magnitude, and Focal Mechanism of the Earthquakes Used in This Study

Event name	Origin time	Latitude	Longitude	Depth (km)	Moment magnitude (Mw)	Strike/rake/dip
Beverly Hills	2012/09/07 T07:03:09.978	34.0660	−118.3983	1.5	3.2	226/−1/80
Westwood	2017/09/19 T06:19:44.368	34.0867	−118.4757	9.0	3.5	85/84/52
Fontana (shallow)	2014/01/15 T09:34:18.868	34.1430	−117.4425	3.5	4.4	44/31/88
Fontana (deep)	2009/01/09 T03:49:46.270	34.1070	−117.3040	15.0	4.3	80/22/70
Chino Hills						
10399801	2009/04/23 T23:56:22.440	33.8946	−117.7971	1.0	3.3	40/−8/83
10399889	2009/04/24 T03:27:50.090	33.8987	−117.7954	2.5	3.6	210/19/84
15207433	2012/08/28 T20:30:59.960	33.9057	−117.7919	6.0	3.9	39/−9/88
15164105	2012/06/14 T03:17:15.240	33.9111	−117.7877	7.0	3.8	131/−174/90
14384236	2008/07/29 T20:40:41.170	33.9393	−117.7536	12.5	3.4	312/171/86

Note. The focal mechanisms of the Beverly Hills-Westwood pair and Fontana pair are determined by the Cut-and-Paste method. The focal mechanisms of Chino Hills series are from the catalog compiled by Wang and Zhan (2020).

on geologic and local soil conditions. For the Beverly Hills-Westwood pair, stations with different site classifications located at the far end of the basin record similarly long shaking durations for the shallow earthquakes and not for the deep earthquakes (Figure S6). This points to the role of common basin path and not individual site effects in the generation of long shaking durations in a basin environment.

The prolonged shaking is also observed for the Fontana pair which sample the three major regional basins (Figure 4). The similarity in waveform between the M3 aftershocks and associated M4 mainshocks shows that the elongated shaking seen more prominently in shallow earthquakes is not due to source complexity but rather the effect of shallow velocity structure. Therefore, understanding the basin response from local

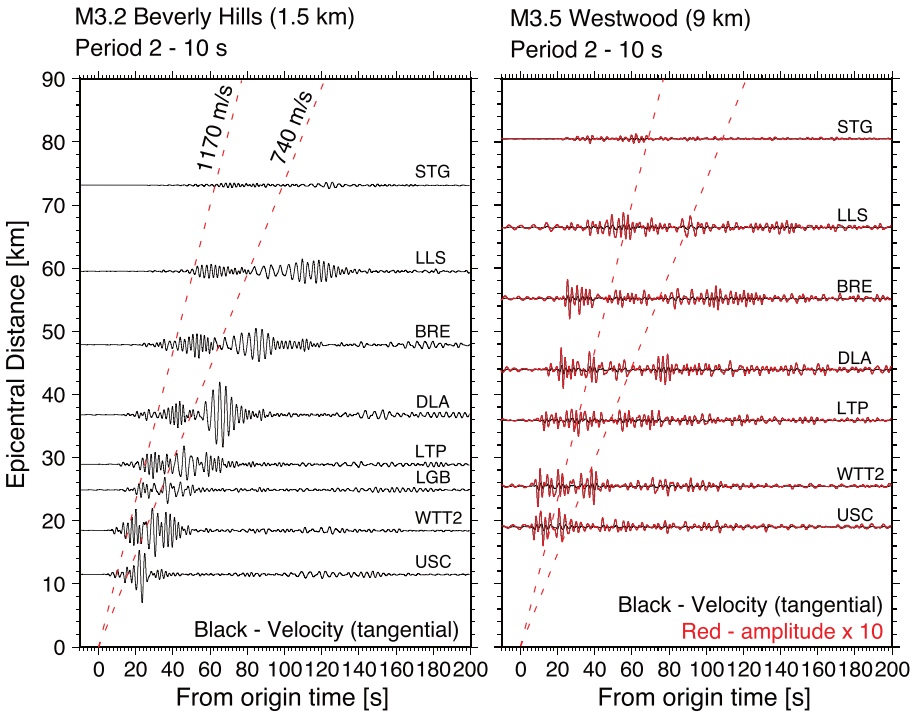

Figure 2. Record sections show the tangential velocity data recorded by stations across the Los Angeles basin for the Beverly Hills (left) and Westwood (right) events. The waveforms are filtered at a period range of 2–10 s and plotted on a common absolute scale. The waveform amplitudes for the Westwood event are significantly weaker; hence for better visuals, the waveforms are scaled by a factor of 10 (shown in red). The dashed red lines indicate the arrivals of initial surface waves and later strong prolonged shaking, traveling at 1,170 and 740 m/s. Similar plots for radial and vertical velocities are in the supporting information.

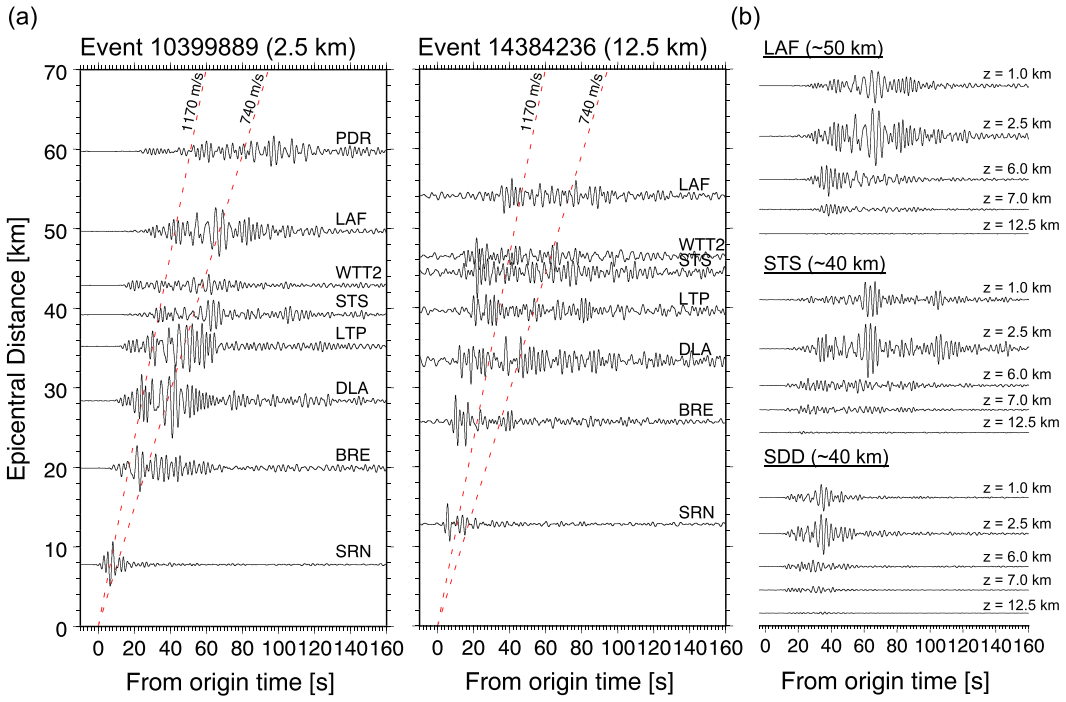

Figure 3. (a) Record sections show the tangential velocity data recorded by stations in the Los Angeles basin for the Chino Hills Events 10399889 at 2.5 km depth (left) and 14384236 at 12.5 km (right). The waveforms are filtered at period 2–10 s, and the amplitudes are scaled using Station SRN. The dashed lines indicate wave packets traveling at 1,170 and 740 m/s, as shown in Figure 2. The record sections for all the events are in the supporting information. (b) Figure shows tangential velocity waveforms recorded at Stations LAF, STS, and SDD amplitudes for all the Chino Hill events. The waveforms are filtered at a period range of 2–10 s, and the amplitudes are scaled by the amplitude at the deepest event (12.5 km). Stations LAF and STS are located near Los Angeles basin, and SDD is to the south, with a travel path completely outside the basin (see exact locations in Figure 1).

shallow earthquakes will be a useful step toward predicting the ground motions, especially waveguide channeling during shallow ruptures at hypothetical large events along the San Andreas fault, as examined in TeraShake (Olsen et al., 2006) and CyberShake (Graves et al., 2011) simulations.

3. Results From 3-D Simulations

Prolonged shaking at periods of 2–5 s can adversely affect tall buildings, bridges, and large-capacity storage tanks in the Los Angeles area as it excites their resonant periods (Wald & Graves, 1998). As physics-based ground motion simulations are used more routinely in seismic hazard analyses, it is vital to validate the performance of predictions from widely used 3-D velocity models CVM-H and CVM-S in terms of predicting the peak acceleration, peak velocity, and shaking duration. These models are considered to be adequate representations of the subsurface structure for at least periods longer than 5 s (Taborda et al., 2016). We focus on modeling the Beverly Hills earthquake as the event is recorded by both broadband and dense nodal arrays and its travel path across the Los Angeles Basin—the edges and shape—is better described due to extensive borehole, seismic reflection, and geologic investigations (e.g., Magistrale et al., 1996; Shaw et al., 2015; Wright, 1991). The small magnitude of the earthquake means it can be treated as a point source for the period range we are investigating.

Using the 3-D finite difference method (Graves, 1996), synthetics accurate up to 1 s period are generated for the 3-D models with a minimum shear wave velocity (V_S) set at 500 m/s and with a 100 m grid spacing. Anelastic attenuation is modeled using the relations $Q_S = 50V_S$ (for V_S in km/s) and $Q_P = 2Q_S$, which are used in previous simulation (e.g., Graves & Pitarka, 2010). Assigning the quality factor (Q_S) to be a function of shear velocity allows the basin, which generally has lower V_S, to have lower Q_S due to the presence of unconsolidated material (Hauksson & Shearer, 2006).

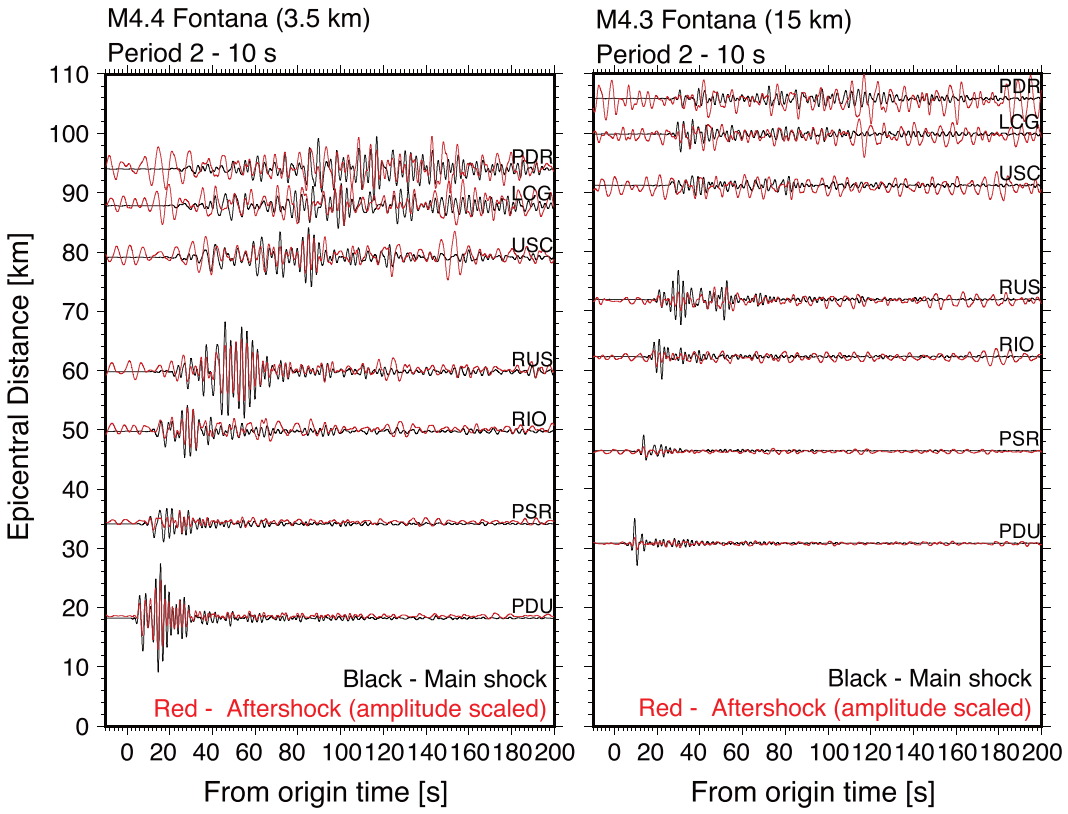

Figure 4. Record sections show the tangential velocity data for the Fontana pair (in black) and their respective M3 aftershocks (in red and scaled with a constant). The waveforms are filtered at a period range of 2–10 s. The station profile is approximately east to west, sampling the San Bernardino, San Gabriel, and Los Angeles basins across the Whittier Narrows (near RUS).

The 3-D simulation results highlight the performance differences of the two CVMs and the underprediction of shaking duration during the shallow events (Figure 5). For the Beverly Hills event, the CVM-S model fits the initial portion of the waveform shape better than CVM-H, in terms of absolute amplitude and period (Figure 5). However, neither model can reproduce the later arriving phases at periods of 2–10 s (Figure 5b). Similarly, the CVM-S model performs better by fitting the first several tens of seconds at periods of 2–10 s for the Fontana pair (Figure S7) and Chino Hills series (Figure S8). This model also reproduces the unusually large ground motions such as Station RUS, which is located in the Whittier Narrows region between the San Gabriel and Los Angeles basins (Figure S7) but does not predict the long shaking duration for most stations within the Los Angeles basin. For the deep Westwood event, which does not exhibit long shaking duration, the CVM-S model is able to fit most of the waveforms over both period ranges.

For CVM-H, the synthetics generally have a poorer waveform fit to the data even at periods of 5–10 s (Figures S9–S11). However, the synthetics contain some late-arriving wave packets (e.g., LTP in Figure 5) which suggests that CVM-H has the appropriate structural configuration to produce late arrivals although the average near-surface velocities are likely too low. Overall, these results are consistent with Taborda et al. (2016) who performed simulations for 30 moderate local events and found that CVM-S produces a consistently higher score based on the goodness-of-fit criteria slightly modified from Anderson (2004) compared to CVM-H at longer periods.

Several factors may contribute to the underprediction of the long duration shaking in our simulations, including the relatively high minimum shear wave velocity in the velocity model and incorrect estimation of event depth. Our test results using the Beverly Hills event in Figure 6 show that these factors do not appear to significantly impact the waveforms or the duration in the period range 2–10 s. Lowering the minimum shear wave velocity of the simulation model from 500 to 250 m/s and using a small grid size of 50 m

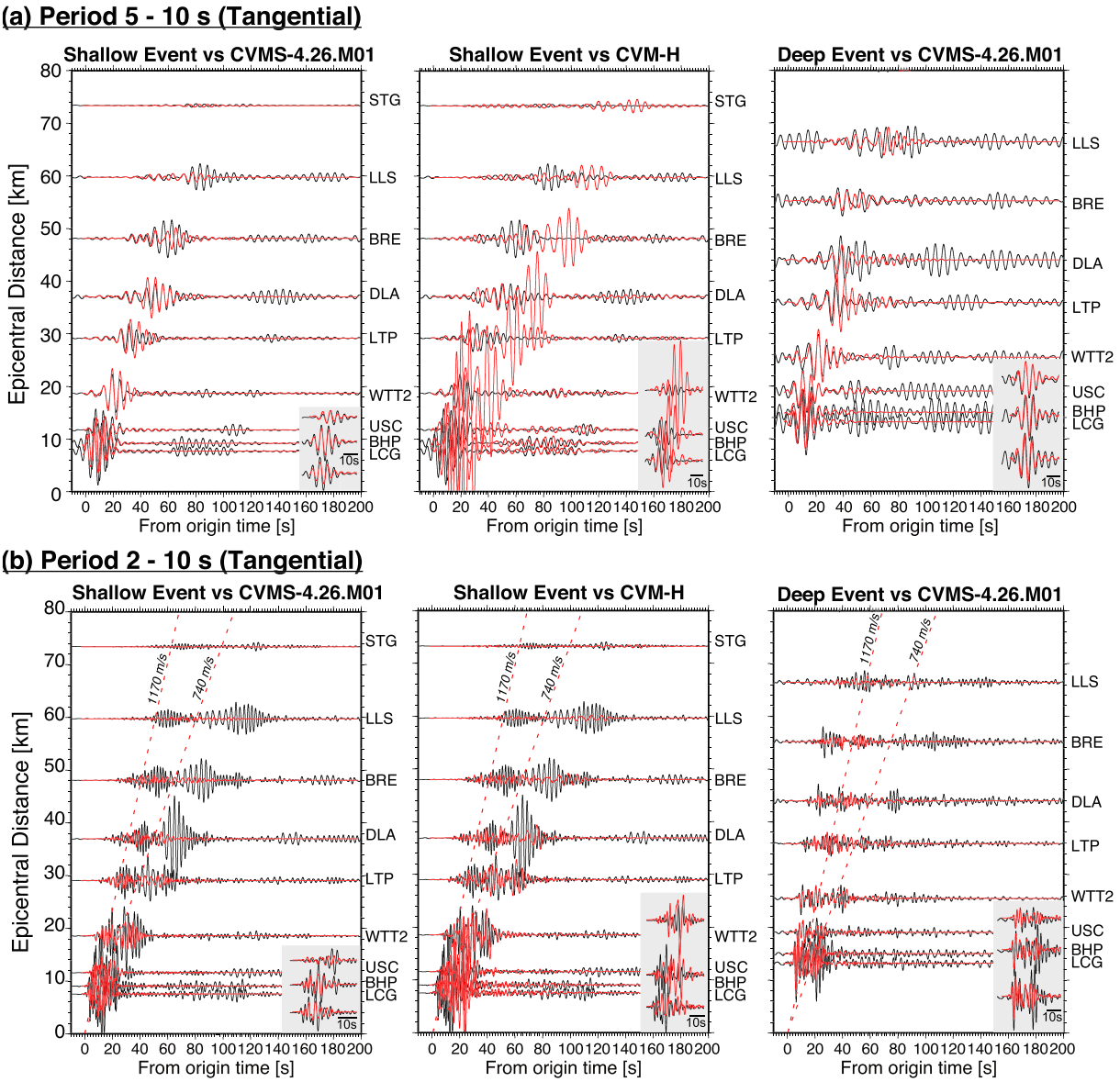

Figure 5. Record sections show the comparison between tangential velocity data (in black) for the Beverly Hills-Westwood pair and the 3-D synthetics (in red) generated from Model CVM-S.4.26.M01 (left and right columns) and CVM-H (middle column). The waveforms are filtered at two different period ranges, 5–10 s (a) and 2–10 s (b). Each section is plotted on a common amplitude scale. The waveforms for the deep event (right column) are multiplied by a factor of 5 as the amplitude is weaker. For visual clarity, the waveforms in the gray box are scaled versions of waveforms at Stations USC (top), BHP (middle), and LCG (bottom). The 3-D synthetics are generated using an attenuation scaling of $Q_S = 50V_S$. Record section of CVM-H synthetics for the Westwood event is in the supporting information.

instead of 100 m reduce the velocity of the shallow-most layers within the basin. However, this implementation produces no significant impact in terms of generating the long duration shaking. Putting the source at a shallower depth (0.5 km instead of 1.5 km) increases the sensitivity to the low velocity shallow layers and thus increases the overall waveform amplitude; but the synthetics overpredict the amplitude of the initial arrivals and, again, do not reproduce the late strong shaking. To ensure the waveform difference is not related to the difference in source mechanism between the Beverly Hills-Westwood pair, we also ran a simulation using a reverse source mechanism (i.e., the same as the Westwood event) and found that it has minimal impact on the waveforms and does not produce the long duration shaking.

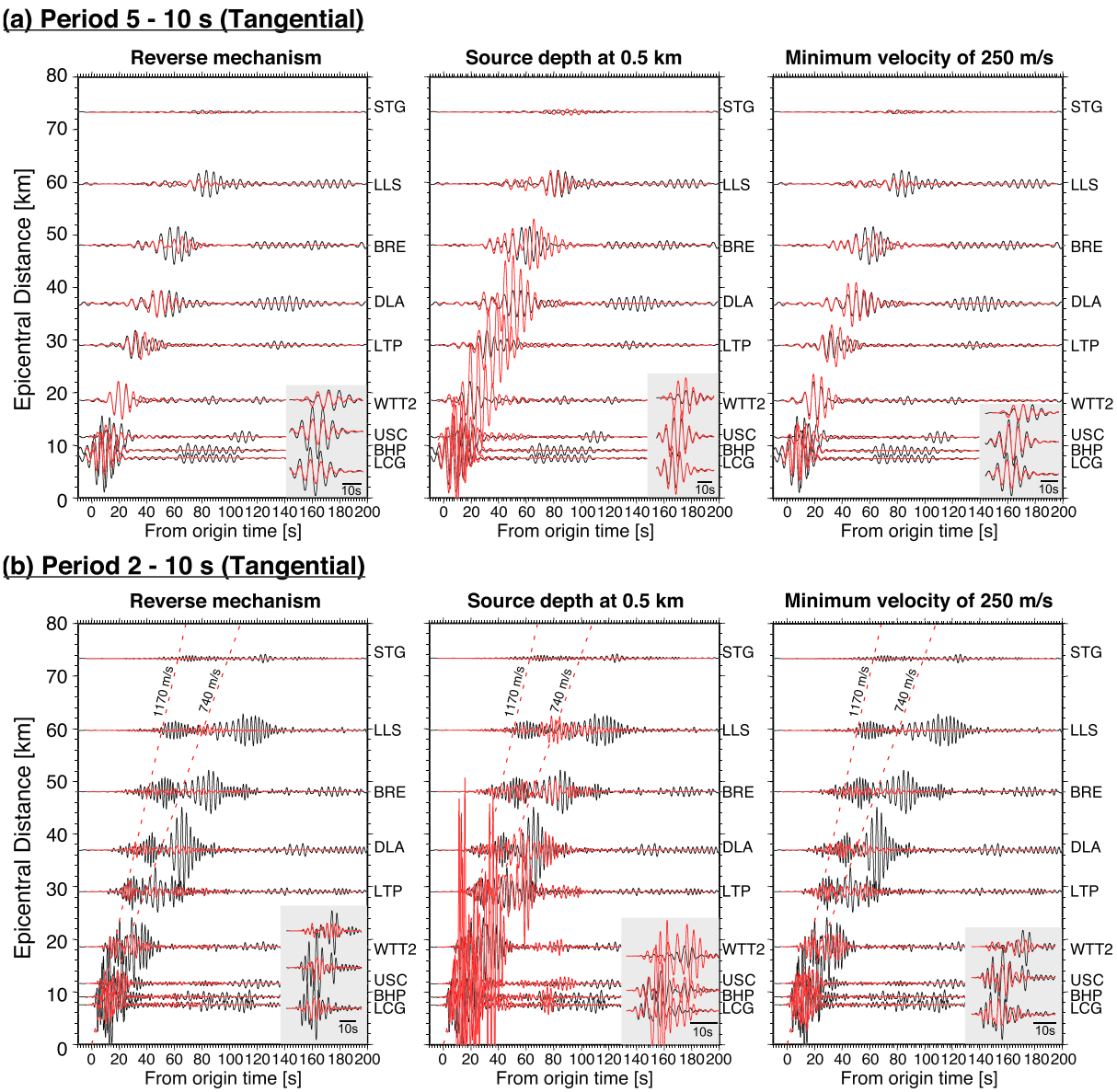

Figure 6. Record sections show the comparison between the tangential velocity data from the Beverly Hills event (black) and the 3-D synthetics generated from CVM-S.4.26.M01 (red) using three different settings: choosing a reverse source mechanism instead of strike-slip (left), setting the source depth at 0.5 km instead of 1.5 km (middle), and using a velocity model with minimum velocity set at 250 m/s instead of 500 m/s. Waveforms are filtered at (a) 5–10 s and (b) 2–10 s and plotted in absolute amplitude. For visual clarity, the waveforms in the gray box are scaled versions of waveforms at Stations USC (top), BHP (middle), and LCG (bottom). The synthetics are generated using an attenuation scaling of $Q_S = 50\ V_S$.

We ran simulations for the Fontana earthquake pair considering other factors such as removing the near-surface GTL at the top 350 m and possible contributions of small-scale stochastic velocity perturbations (Figure S12). For the simulation without the near-surface low-velocity GTL at the top 350 m, the waveform fits for certain stations like PSR and RUS worsen, but for stations like USC and LCG, they are mildly improved. However, there is little effect on the durations of the motions for the shallow source. Adding stochastic perturbations to the velocity structure (e.g., Graves & Pitarka, 2016) can promote scattering, which may increase the shaking duration, but we observe that this does not significantly improve the fitting at this period range.

On the other hand, we find that the choice of anelastic attenuation factors has a strong impact on the modeled duration. With stronger attenuation, energy at shorter periods (<5 s) decays more rapidly with time. Lin

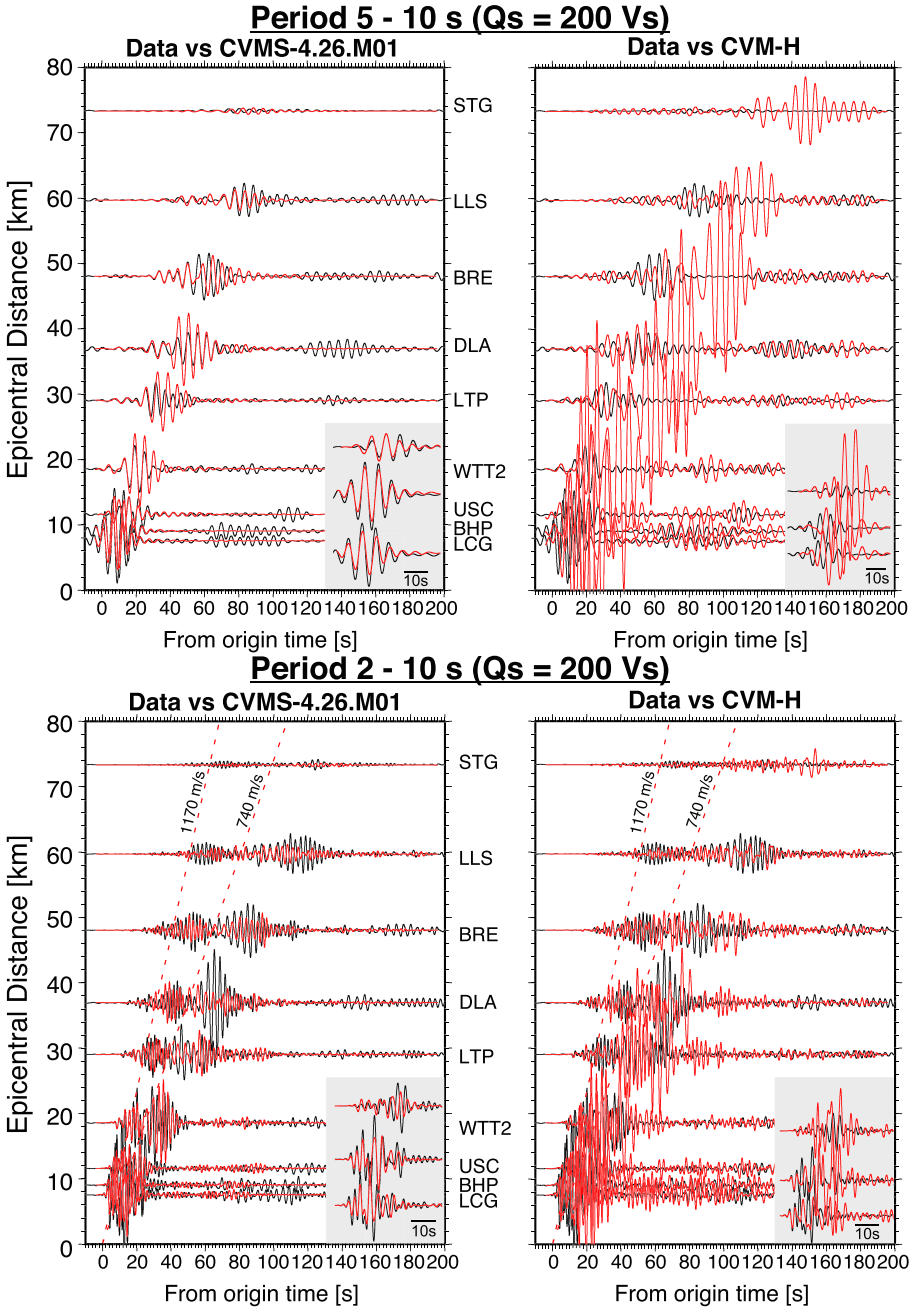

Figure 7. Record sections show the comparison between tangential velocity data (in black) for the Beverly Hills event and 3-D synthetics (in red) generated from Model CVM-S.4.26.M01 (left column) and CVM-H (right column). The waveforms are filtered at a period range 5–10 s (top row) and 2–10 s (bottom row). The 3-D synthetics are generated using a weaker attenuation scaling of $Q_S = 200\ V_S$. For visual clarity, the waveforms in the gray box are scaled versions of waveforms at Stations USC (top), BHP (middle), and LCG (bottom).

and Jordan (2018) suggested that the attenuation scaling ($Q_S = 50\ V_S$) used in earthquake simulations are four times weaker than observed in t* measurements by Hauksson and Shearer (2006) for frequencies of 2–30 Hz. When weaker attenuation scaling is used ($Q_S = 200\ V_S$), we observed that more energy is preserved, and waveform fitting especially for the earlier wave packet has improved (Figure 7). At 5–10 s, the weaker attenuation improves the fit to the later arrivals produced by CVM-S (e.g., Station LLS) but significantly overestimates the amplitude of the later arrivals for CVM-H. At 2–10 s, both models produce

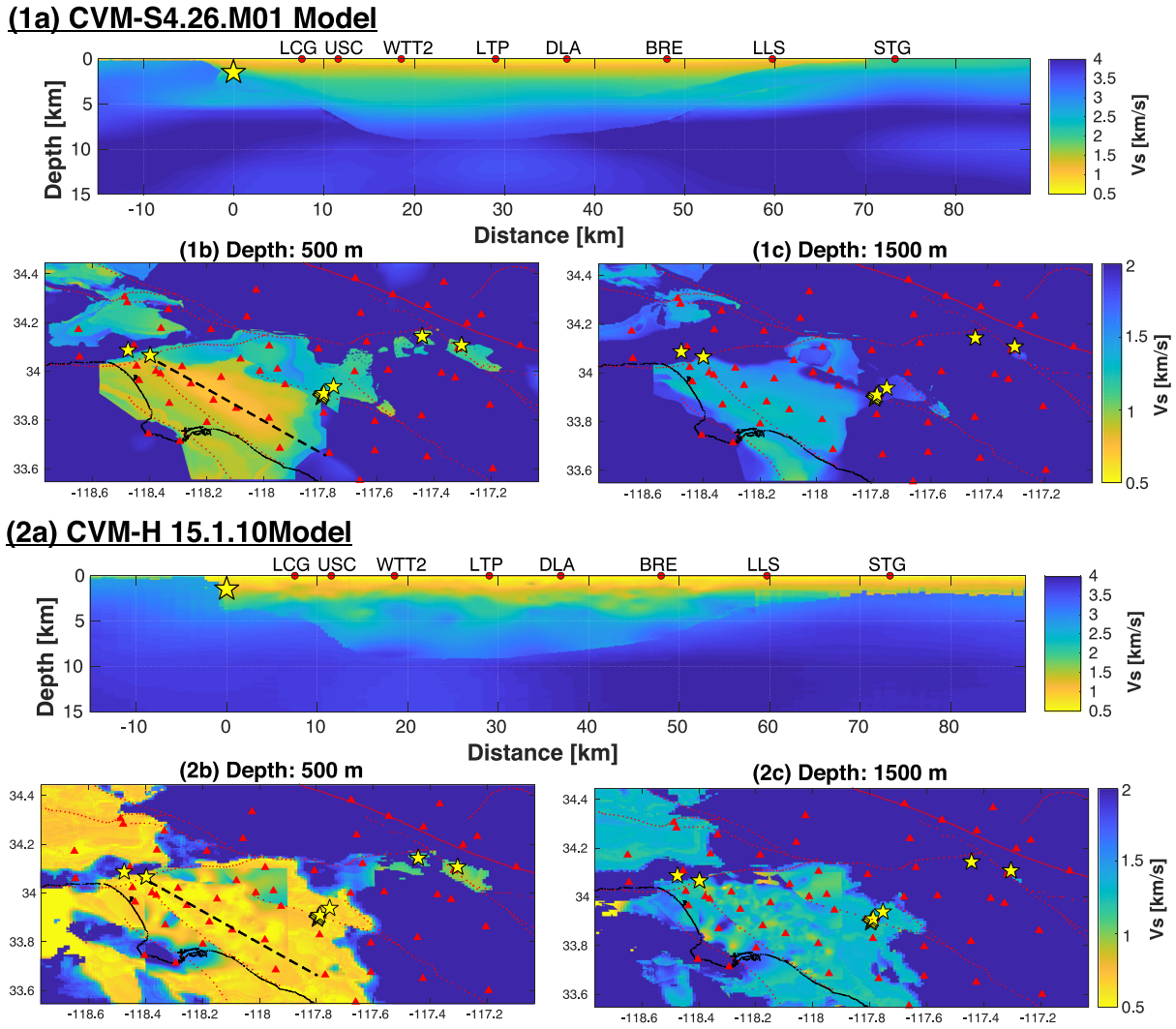

Figure 8. (top panel, 1a) Cross section showing the shear wave velocity structure from the CVM-S4.26.M01 model across the Los Angeles Basin, stations (red) along the profile, and the depth of the 2012 Beverly Hills shallow event (yellow star). Maps show horizontal depth profile of the CVM-S4.26.M01 model at depth 500 m (1b) and 1,500 m (1c). The black dashed line shows the location of the cross-section profile. Locations of earthquakes (yellow stars) and seismometers (red triangles) are shown as well. Red lines delineate the known regional faults (Jennings, 1994). (bottom panel, 2a–2c) Similar cross section and maps but for the CVM-H15.1.0 model.

some late arriving waves; however, neither model is able to adequately match the amplitude or phasing of the observed waveforms. A comparison of Q_S with different scaling factors (50 V_S, 100 V_S, and 200 V_S) for CVM-S are shown in Figure S13. In this study, we do not prescribe the best fitting attenuation model but rather simply point out that the choice of attenuation model has a strong effect in modulating shaking duration for shallow sources, possibly allowing better fits to the waveform data.

In short, the synthetics from 3-D velocity model CVM-S can reproduce most of the initial phases better than the synthetics from CVM-H. The CVM-H model can produce the later arriving 5–10 s period waves, although they are larger in amplitude and delayed relative to the observations. With weaker attenuation, both models produce longer durations, although neither model fits well the phasing of the observed waveforms at periods of 2–10 s.

The differences seen in the synthetics from the two CVMs stem from variations in the shallow geologic structures in the models (Figure 8). In CVM-S, the entire model has been updated using waveform tomography, which has a lower-period passband bound of about 5 s (Lee et al., 2014). The result is that the velocity structure of CVM-S is smoothly varying, so any sharp velocity contrasts from the original model have been

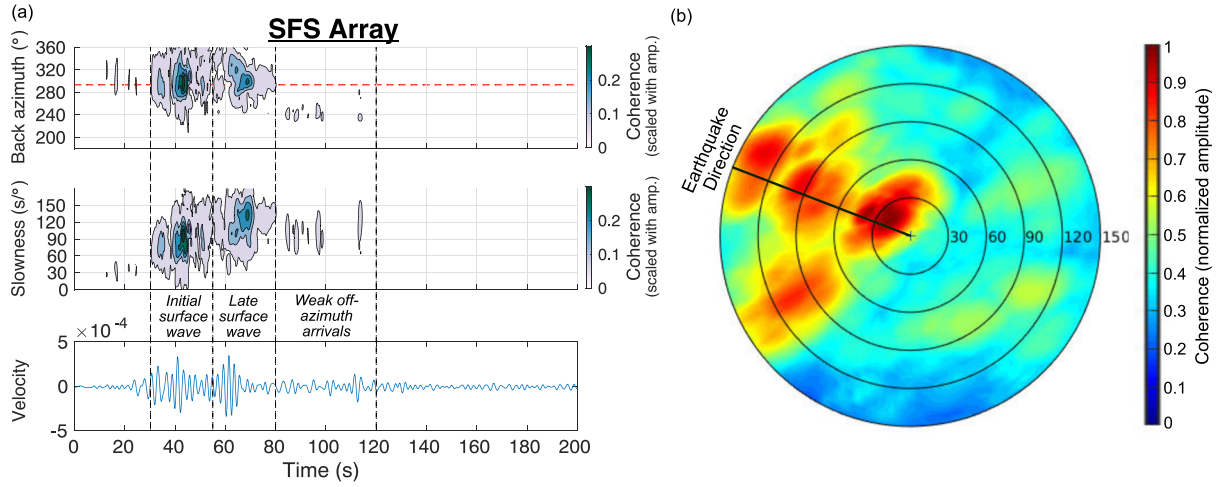

Figure 9. (a) The back azimuth and slowness of *P*, *S*, and surface wave arrivals from the Beverly Hills event at the Santa Fe Springs (SFS) array located 35.5 km away from the epicenter. The coherence is scaled with amplitude to highlight stronger shaking. The earthquake is at a back azimuth of 291 degrees. The vertical-component velocity seismogram recorded by one of the stations in the center of the SFS array is also shown. The seismogram is band-pass filtered between 2 and 10 s with a two-pass Butterworth filter. (b) Polar plots showing the data coherence, stacked over the entire 200 s duration. The amplitude is normalized in order to show the weak yet coherent arrivals. Warmer color indicates higher coherence. Most coherent energy is confined to the great circle path. There is some coherent energy observed arriving from off-great circle azimuths at times of 80 to 120 s.

blurred out. Without sharp, shallow basin edges, this model does not produce strong converted basin surface waves for shallow events, particularly for periods below 5 s. While CVM-H15.1.0 has also undergone tomographic updates, the basin structures have been reinserted, so that the shallow, detailed heterogeneities from the original model are preserved. This structure generates strong basin surface waves for shallow events, such as those seen at 5–10 s period in Figure 5. However, these later arrivals travel with a slower apparent velocity than seen in the data, suggesting that the shallow velocities in CVM-H may be too low. Additionally, the presence of lateral heterogeneities within the shallow basin sediments of CVM-H breaks up the coherence of the prolonged shaking across the basin at periods below 5 s. The following section explores the role of shallow heterogeneities in the wave propagation by tracking the propagation directions of the wavefront using data with a dense array.

4. Beamforming Analysis on Dense Array

Array processing techniques, when applied to dense array deployments, can be used to estimate the propagation direction, slowness, and arrival time of each coherent wavefront passing across the sensors. These techniques have been used extensively to study the fine-scale structure of the Earth's interior (e.g., Rost & Thomas, 2002) and recently have been applied at a regional scale by Yu et al. (2017) who used these techniques to identify prominent scatterers within the upper crust, such as the bathymetric relief in the Southern California Continental Borderland. The shallow Beverly Hills event is recorded by the Santa Fe Springs (SFS) array (Figure 1), a particularly dense deployment of single vertical-component FairField Node sensors, which provides a unique opportunity to investigate how the path across the Los Angeles basin enables long duration shaking. The SFS array consisted of 1,464 sensors at the time of the earthquake, with a sensor spacing averaging 100 m. Data with a low signal-to-noise ratio and no visible earthquake signals were removed, retaining 97% of the SFS array data. The instrument response is removed from the data.

To detect how a seismic wavefield travels across an array, we use the phase stack (or phase coherence) method, as described in Schimmel and Paulssen (1997) and implemented in Yu et al. (2017). In the phase stack method, the seismic traces are first converted into analytic traces using Hilbert transform, and the phase is retained while the amplitudes of the traces are normalized to unity sample by sample. The phase coherence is then measured by averaging these analytic traces in the complex plane. Using phase coherence measurements allows us to detect weak but coherent locally plane-wave signals arriving at the array at a range of incident azimuths and slownesses, some of which are due to seismic scattering. The

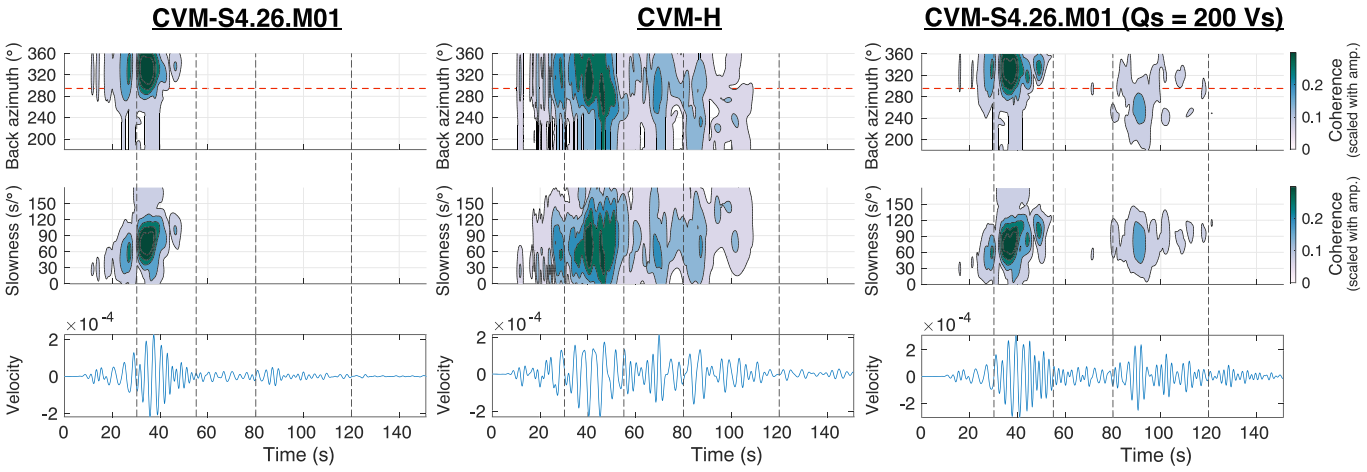

Figure 10. Plots show the back azimuth and slowness of *P*, *S*, and surface wave synthetic arrivals from the Beverly Hills event at Santa Fe Springs (SFS) array generated using Model CVM-S4.26.M01 (Qs = 50 Vs), CVM-H, and CVM-S4.26.M01 (Qs = 200 Vs). The coherence is scaled with amplitude to highlight stronger shaking. The seismogram is band-pass filtered between 2 and 10 s with a two-pass Butterworth filter. The dashed lines indicate the different surface wave packets seen in the data (Figure 8).

phase coherence can later be scaled with the amplitude to emphasize coherent arrivals that are strong in amplitude, in this case, significant shaking.

At a period of 2–10 s, the SFS array shows several arrivals of coherent energy with increasing slowness corresponding to *P* waves, *S* waves, and surface waves (Figure 9). When scaled with amplitude, the strong surface wave shaking across the SFS array lasts up to 50 s (at timestamp of 30–80 s). The prolonged shaking travels with slowness up to 150 s/deg (=740 m/s) and arrives from the same azimuth as the direction from the earthquake epicenter, that is, the energy is traveling along the great circle path, rejecting the idea that the prolonged shaking is due to off-azimuth basin reverberations. The difference in slowness of the later arrivals (150 s/deg) compared to the first packet of surface waves (100 s/deg) also indicates that the later surface waves are sampling very slow structures not sampled by the initial surface wave packet.

Interestingly, there is a stream of very weak yet coherent energy recorded at the SFS array traveling at the same slowness of 100 s/deg and arriving from an off-great circle azimuth of 240 deg at in the later time window of 80–120 s. Assuming constant slowness, we can estimate that some energy from the earthquake is scattered offshore, near the edge of the Santa Cruz Basin along the Inner Borderland, and reached the array as a coherent late arrival. The estimated scattering location has a pronounced topographic relief and showed prominent scattering in the case of teleseismic SH waves (Yu et al., 2017). This weak late arrival can be observed at other stations, arriving about 40 s after the surface wave train and are more pronounced at longer period (Figure 5).

We also performed similar beamforming analysis using three different models, that is, CVM-S, CVM-H, and CVM-S with weaker attenuation (Figure 10). Despite suffering from some smearing of energy resulting in less accurate back-azimuth measurements, this analysis confirms that the synthetics from the three models can match the initial surface wave and its slowness but do not produce the late strong shaking with high slowness. Synthetics from the CVM-H model further show many coherent late arrivals from a wide range of back azimuths, traveling at the same velocity of the initial surface wave. These arrivals probably arise from reflections off regional heterogeneities such as slow pockets within basins and offshore structures which are preserved in the CVM-H model (Figure 8). Late, off-azimuth arrivals are also observed in the CVM-S model with weaker attenuation; however, these are likely artifacts due to reflections from the imposed boundary of the regional basin structure (see Figures 8b and 8c).

5. Discussion

Understanding how waves propagate in sedimentary basins is important for ground motion prediction. Basin environments with large velocity jump along the basin edges can create surface waves with fundamental and

higher modes, which has been observed in many sedimentary basins including the Kanto basin in Japan (Boué et al., 2016) and the Valley of Mexico in Mexico (Cruz-Atienza et al., 2016). We propose that in the Los Angeles basin, the prolonged shaking observed during shallow earthquakes is due to effective generation of the basin surface waves at the basin edges. This strong late shaking develops coherently across the basin, starting from the station closest to the basin edge. For paths outside the basin, the late shaking is not seen. This phenomenon is particularly strong in a period band of 2–10 s, potentially posing an increased risk to tall buildings, bridges, and large-capacity storage tanks in the Los Angeles area. One possible reason for the depth-dependent behavior is that at shallower depths, the velocity contrast across the basin edge is larger, hence allowing a higher transmission of surface wave energy into the basin (Brissaud et al., 2020).

The beamforming results further show that late shaking is not caused by off-azimuth basin reverberations but is dominated by a surface wave that travels at high slowness from the back azimuth of the earthquake. Based on particle motion using radial and vertical components, the late surface wave is retrograde, which is identified as the fundamental mode by Ma et al. (2016) using ambient noise cross-correlations in Los Angeles basin. Given that the fundamental mode is most sensitive to near-surface layers (Rivet et al., 2015), this mode traveling with high slowness indicates the role of shallow basin-edge structure and low seismic velocities within the basin in exciting long shaking durations, consistent with previously proposed hypotheses (e.g., Kawase & Aki, 1989).

To improve the performance of physics-based forward simulations and to better constrain shear wave velocity models, it is important to resolve the attenuation model in the shallow crust. In most numerical waveform simulations, intrinsic attenuation is applied using a scaling law that is a function of V_S (Olsen et al., 2006; Taborda et al., 2016). Such scaling implies the strongest attenuation occurs near the surface within the basin structure, as there the velocity values are typically the lowest. Using the conventional relation of $Q_S = 50\ V_S$ means the top 1 km layer has an average Q_S of 50–100. This relation is consistent with the Q_S values proposed in Hauksson and Shearer (2006) and is higher than prescribed in Olsen et al. (2003) where $Q_S = 20\ V_S$ for $V_S < 2$ km/s (Figure S14). Our simulation results show that the choice of scaling strongly affects the surface waves as they are sensitive to the slow shallow layers in the velocity model. Implementing a weaker attenuation relation (i.e., larger Q_S) will reproduce some of the prolonged shaking at 2 s (Figure 7).

However, weak attenuation alone is insufficient to predict the waveform. The beamforming results highlight that the shallow layers are crucial in producing the late strong shaking, but they are not well described in the current 3-D CVMs. For instance, the CVM-H model has sharp basin edges and thick, slow layers near the surface (Figure 8), which creates a strong late wave train, but the amplitude is overpredicted compared to observations. On the other hand, the current version of CVM-S can fit the first tens of seconds of the longer period waveforms well for a majority of events and capture the local variation of ground motion amplification. Regional structures such as shallow basin heterogeneities in CVM-H and sharp offshore boundaries in CVM-S can also mimic the observed off-azimuth arrivals. Future improvements to simulations using 3-D velocity models should consider (1) a more accurate representation of shallow heterogeneities and seismic velocities within the Los Angeles basin along with preserving basin edge information and (2) an appropriate shallow velocity and attenuation scaling model. Improvements in station coverage, either with seismic instruments or other novel sensors such as a distributed acoustic sensing system (e.g., Zhan, 2020), will increase our ability to image shallow heterogeneities and velocity structure in the basin.

6. Conclusion

By using several groups of small-magnitude, shallow, and deep earthquakes recorded across the Los Angeles basin, we found that shallow events generate longer shaking durations at the period range of 2–10 s than deeper events. The coherence of the wave train observed with a beamforming analysis suggests that the basin edges are responsible for exciting the long shaking duration through surface wave generation. Additional late but weaker surface waves arriving off-azimuth are potentially scattered by regional structures. Current 3-D CVMs in their present form do not accurately predict the observed long shaking durations. Possible modifications to these models, including more accurate imaging of basin edges and shallow heterogeneities within the basins and better constraints on the shallow velocity and attenuation structure, will likely lead to improved modeling of these basin-generated phases.

Data Availability Statement

All waveform data were accessed through the Southern California Earthquake Data Center (SCEDC) at Caltech (https://doi.org/10.7909/C3WD3xH1). The community velocity models are obtained through the UCVM software framework maintained by Southern California Earthquake Center (Small et al., 2017).

Acknowledgments
This work is supported by Southern California Earthquake Center grant (#18128). The computations presented here were conducted on the Caltech High Performance Cluster, partially supported by a grant from the Gordon and Betty Moore Foundation. We appreciate feedback from Carl Tape, Grace Parker, Elizabeth Cochran, associate editor, and an anonymous reviewer which greatly improved the manuscript. Several plots were made using the Generic Mapping Tools Version 4.2.1 (www.soest.hawaii.edu/gmt; Wessel & Smith, 1998). We thank Rob Clayton for his assistance in acquiring the dense array data set and Breitburn Energy Partners for the usage of the Santa Fe Springs dense array data set.

References

Anderson, J. G. (2004). *Quantitative measure of the goodness-of-fit of synthetic seismograms* (Vol. 243). Paper presented at 13th World Conference on Earthquake Engineering Conference Proceedings, Vancouver, Canada.

Boué, P., Denolle, M., Hirata, N., Nakagawa, S., & Beroza, G. C. (2016). Beyond basin resonance: Characterizing wave propagation using a dense array and the ambient seismic field. *Geophysical Journal International*, *206*, 1261–1272. https://doi.org/10.1093/gji/ggw205

Bowden, D. C., & Tsai, V. C. (2017). Earthquake ground motion amplification for surface waves. *Geophysical Research Letters*, *44*, 121–127. https://doi.org/10.1002/2016GL071885

Brissaud, Q., Bowden, D. C., & Tsai, V. C. (2020). Extension of the basin Rayleigh-wave amplification theory to include basin-edge effects. *Bulletin of the Seismological Society of America*, *110*, 1305–1322. https://doi.org/10.1785/0120190161

Cruz-Atienza, V. M., Tago, J., Sanabria-Gómez, J. D., Chaljub, E., Etienne, V., Virieux, J., & Quintanar, L. (2016). Long duration of ground motion in the paradigmatic valley of Mexico. *Scientific Reports*, *6*, 38807. https://doi.org/10.1038/srep38807

Day, S. M., Graves, R., Bielak, J., Dreger, D., Larsen, S., Olsen, K. B., et al. (2008). Model for basin effects on long-period response spectra in southern California. *Earthquake Spectra*, *24*(1), 257–277. https://doi.org/10.1193/1.2857545

Ely, G. P., Jordan, T. H., Small, P., & Maechling, P. J. (2010, December). *A V_{S30}-derived near-surface seismic velocity model* (Vol. S51A-1907). Paper presented at AGU 2010 Fall Meeting, American Geophysical Union: San Francisco, CA.

Graves, R., Jordan, T. H., Callaghan, S., Deelman, E., Field, E., Juve, G., et al. (2011). CyberShake: A physics-based seismic hazard model for southern California. *Pure and Applied Geophysics*, *168*(3–4), 367–381. https://doi.org/10.1007/s00024-010-0161-6

Graves, R. W. (1996). Simulating seismic wave propagation in 3D elastic media using staggered-grid finite differences. *Bulletin of the Seismological Society of America*, *86*(4), 1091–1106.

Graves, R. W., & Pitarka, A. (2010). Broadband ground-motion simulation using a hybrid approach. *Bulletin of the Seismological Society of America*, *100*(5A), 2095–2123. https://doi.org/10.1785/0120100057

Graves, R. W., & Pitarka, A. (2016). Kinematic ground-motion simulations on rough faults including effects of 3D stochastic velocity perturbations. *Bulletin of the Seismological Society of America*, *106*, 2136–2153. https://doi.org/10.1785/0120160088

Graves, R. W., Pitarka, A., & Somerville, P. G. (1998). Ground-motion amplification in the Santa Monica area: Effects of shallow basin-edge structure. *Bulletin of the Seismological Society of America*, *88*(5), 1224–1242.

Hauksson, E., & Shearer, P. M. (2006). Attenuation models (QP and QS) in three dimensions of the southern California crust: Inferred fluid saturation at seismogenic depths. *Journal of Geophysical Research*, *111*, B05302. https://doi.org/10.1029/2005JB003947

Hauksson, E., Yang, W., & Shearer, P. M. (2012). Waveform relocated earthquake catalog for southern California (1981 to June 2011). *Bulletin of the Seismological Society of America*, *102*(5), 2239–2244. https://doi.org/10.1785/0120120010

Hruby, C. E., & Beresnev, I. A. (2003). Empirical corrections for basin effects in stochastic ground-motion prediction, based on the Los Angeles basin analysis. *Bulletin of the Seismological Society of America*, *93*(4), 1679–1690. https://doi.org/10.1785/0120020121

Jennings, C. W. (1994). Fault activity map of California and adjacent areas, with locations and ages of recent volcanic eruptions California Department of Conservation, Division of Mines and Geology. Geologic Data Map No. 6.

Kawase, H. (1996). The cause of the damage belt in Kobe: "The basin-edge effect," constructive interference of the direct S-wave with the basin-induced diffracted/Rayleigh waves. *Seismological Research Letters*, *67*(5), 25–34. https://doi.org/10.1785/gssrl.67.5.25

Kawase, H., & Aki, K. (1989). A study on the response of a soft basin for incident S, P, and Rayleigh waves with special reference to the long duration observed in Mexico City. *Bulletin of the Seismological Society of America*, *79*(5), 1361–1382.

Komatitsch, D., Liu, Q., Tromp, J., Suss, P., Stidham, C., & Shaw, J. H. (2004). Simulations of ground motion in the Los Angeles basin based upon the spectral-element method. *Bulletin of the Seismological Society of America*, *94*(1), 187–206. https://doi.org/10.1785/0120030077

Lee, E. J., Chen, P., Jordan, T. H., Maechling, P. B., Denolle, M. A., & Beroza, G. C. (2014). Full-3-D tomography for crustal structure in southern California based on the scattering-integral and the adjoint-wavefield methods. *Journal of Geophysical Research: Solid Earth*, *119*, 6421–6451. https://doi.org/10.1002/2014JB011346

Lee, S. J., Chen, H. W., Liu, Q., Komatitsch, D., Huang, B. S., & Tromp, J. (2008). Three-dimensional simulations of seismic-wave propagation in the Taipei basin with realistic topography based upon the spectral-element method. *Bulletin of the Seismological Society of America*, *98*(1), 253–264. https://doi.org/10.1785/0120070033

Lin, Y. P., & Jordan, T. H. (2018). Frequency-dependent attenuation of P and S waves in Southern California. *Journal of Geophysical Research: Solid Earth*, *123*, 5814–5830. https://doi.org/10.1029/2018JB015448

Lui, S. K., Helmberger, D., Yu, J., & Wei, S. (2016). Rapid assessment of earthquake source characteristics. *Bulletin of the Seismological Society of America*, *106*, 2490–2499. https://doi.org/10.1785/0120160112

Ma, Y., Clayton, R. W., & Li, D. (2016). Higher-mode ambient-noise Rayleigh waves in sedimentary basins. *Geophysical Journal International*, *206*, 1634–1644. https://doi.org/10.1093/gji/ggw235

Magistrale, H., McLaughlin, K., & Day, S. (1996). A geology-based 3D velocity model of the Los Angeles basin sediments. *Bulletin of the Seismological Society of America*, *86*(4), 1161–1166.

Moschetti, M. P., Thompson, E. M., Rekoske, J., Hearne, M. G., Powers, P. M., McNamara, D. E., & Tape, C. (2019). Ground-motion amplification in Cook Inlet Region, Alaska, from intermediate-depth earthquakes, including the 2018 M_w 7.1 Anchorage earthquake. *Seismological Research Letters*, *91*, 142–152.

Olsen, K. B., Day, S. M., & Bradley, C. R. (2003). Estimation of Q for long-period (>2 sec) waves in the Los Angeles Basin. *Bulletin of the Seismological Society of America*, *93*(2), 627–638. https://doi.org/10.1785/0120020135

Olsen, K. B., Day, S. M., Minster, J. B., Cui, Y., Chourasia, A., Faerman, M., et al. (2006). Strong shaking in Los Angeles expected from southern San Andreas earthquake. *Geophysical Research Letters*, *33*, L07305. https://doi.org/10.1029/2005GL025472

Rivet, D., Campillo, M., Sanchez-Sesma, F., Shapiro, N. M., & Singh, S. K. (2015). Identification of surface wave higher modes using a methodology based on seismic noise and coda waves. *Geophysical Journal International*, *203*, 856–868. https://doi.org/10.1093/gji/ggv339

Rost, S., & Thomas, C. (2002). Array seismology: Methods and applications. *Reviews of Geophysics*, *40*(3), 1008. https://doi.org/10.1029/2000rg000100

Saikia, C. K., Dreger, D. S., & Helmberger, D. V. (1994). Modeling of energy amplification recorded within greater Los Angeles using irregular structure. *Bulletin of the Seismological Society of America*, *84*(1), 47–61.

Schimmel, M., & Paulssen, H. (1997). Noise reduction and detection of weak, coherent signals through phase-weighted stacks. *Geophysical Journal International*, *130*(2), 497–505. https://doi.org/10.1111/j.1365-246X.1997.tb05664.x

Shaw, J. H., Plesch, A., Tape, C., Suess, M. P., Jordan, T. H., Ely, G., et al. (2015). Unified structural representation of the southern California crust and upper mantle. *Earth and Planetary Science Letters*, *415*, 1–15. https://doi.org/10.1016/j.epsl.2015.01.016

Small, P., Gill, D., Maechling, P. J., Taborda, R., Callaghan, S., Jordan, T. H., et al. (2017). The SCEC unified community velocity model software framework. *Seismological Research Letters*, *88*, 1539–1552. https://doi.org/10.1785/0220170082

Süss, M. P., & Shaw, J. H. (2003). P wave seismic velocity structure derived from sonic logs and industry reflection data in the Los Angeles basin, California. *Journal of Geophysical Research*, *108*(B3), 2170. https://doi.org/10.1029/2001JB001628

Taborda, R., Azizzadeh-Roodpish, S., Khoshnevis, N., & Cheng, K. (2016). Evaluation of the southern California seismic velocity models through simulation of recorded events. *Geophysical Journal International*, *205*, 1342–1364. https://doi.org/10.1093/gji/ggw085

Wald, D. J., & Graves, R. W. (1998). The seismic response of the Los Angeles basin, California. *Bulletin of the Seismological Society of America*, *88*(2), 337–356.

Wang, X., & Zhan, Z. (2020). Moving from 1-D to 3-D velocity model: Automated waveform-based earthquake moment tensor inversion in the Los Angeles region. *Geophysical Journal International*, *220*, 218–234. https://doi.org/10.1093/gji/ggz435

Wessel, P., & Smith, W. H. F. (1998). New, improved version of generic mapping tools released. *Eos, Transactions American Geophysical Union*, *79*(47), 579–579. https://doi.org/10.1029/98eo00426

Wirth, E. A., Vidale, J. E., Frankel, A. D., Pratt, T. L., Marafi, N., Thompson, M., & Stephenson, W. J. (2019). Source-dependent amplification of earthquake ground motions in deep sedimentary basins. *Geophysical Research Letters*, *46*, 6443–6450. https://doi.org/10.1029/2019GL082474

Wright, T. L. (1991). Structural geology and tectonic evolution of the Los Angeles Basin, California: Chapter 3: Part 1.

Yu, C., Zhan, Z., Hauksson, E., & Cochran, E. S. (2017). Strong SH-to-love wave scattering off the Southern California continental borderland. *Geophysical Research Letters*, *44*, 10,208–10,215. https://doi.org/10.1002/2017GL075213

Zhan, Z. (2020). Distributed acoustic sensing turns fiber-optic cables into sensitive seismic antennas. *Seismological Research Letters*, *91*, 1–15. https://doi.org/10.1785/0220190112

Zhao, L. S., & Helmberger, D. V. (1994). Source estimation from broadband regional seismograms. *Bulletin of the Seismological Society of America*, *84*(1), 91–104.

Zhu, L., & Helmberger, D. V. (1996). Advancement in source estimation techniques using broadband regional seismograms. *Bulletin of the Seismological Society of America*, *86*(5), 1634–1641.

Zhu, L., & Zhou, X. (2016). Seismic moment tensor inversion using 3D velocity model and its application to the 2013 Lushan earthquake sequence. *Physics and Chemistry of the Earth, Parts A/B/C*, *95*, 10–18. https://doi.org/10.1016/j.pce.2016.01.002

References From the Supporting Information

Brocher, T. M. (2008). Compressional and shear-wave velocity versus depth relations for common rock types in northern California. *Bulletin of the Seismological Society of America*, *98*(2), 950–968. https://doi.org/10.1785/0120060403

Yong, A., Thompson, E. M., Wald, D., Knudsen, K. L., Odum, J. K., Stephenson, W. J., & Haefner, S. (2016). *Compilation of V_{S30} data for the United States: U.S. Geological Survey Data Series 978* (pp. 1–8). https://doi.org/10.3133/ds978